



Sinking enhances the degradation of organic particles by marine bacteria

Uria Alcolombri¹✉, François J. Peauderf¹, Vicente I. Fernandez¹, Lars Behrendt^{1,2}, Kang Soo Lee¹ and Roman Stocker¹✉

The sinking of organic particles in the ocean and their degradation by marine microorganisms is one of the main drivers of the biological pump. Yet, the mechanisms determining the magnitude of the pump remain poorly understood, limiting our ability to predict this carbon flux in future ocean scenarios. Current ocean models assume that the biological pump is governed by the competition between sinking speed and degradation rate, with the two processes independent from one another. Contrary to this paradigm, we show that sinking itself is a primary determinant of the rate at which bacteria degrade particles. Heterotrophic bacterial degradation rates were obtained from a laboratory study on model surface-colonized particles at atmospheric pressure under a range of flow speeds to mimic different sinking velocities. We find that even modest sinking speeds of 8 m day⁻¹ enhance degradation rates more than 10-fold compared with degradation rates of non-sinking particles. We discovered that the molecular mechanism underlying this sinking-enhanced degradation is the flow-induced removal from the particles of the oligomeric breakdown products, which otherwise compete for enzymatic activity. This mechanism applies across several substrates and bacterial strains, suggesting its potentially broad occurrence under natural marine conditions. Integrating our findings into a mathematical model of particulate carbon flux, we propose that the coupling of sinking and degradation may contribute, in conjunction with other processes, to determining the magnitude of the vertical carbon flux in the ocean.

The biological pump is the process by which CO₂ from the atmosphere is converted by marine photosynthetic organisms into biomass and inorganic carbonate shells and is then sequestered in the ocean depths when those organisms die and aggregate to form ‘marine snow’ particles that sink^{1–7}. The sinking of particles and the vertical export of the carbon present in marine snow is affected by complex interactions between physical, chemical and biological processes that vary in magnitude with site, depth and season. These processes include zooplankton particle consumption and excretion^{1,2,8}, zooplankton vertical migration^{1,2}, particle aggregation and fragmentation⁹ and degradation by marine bacteria¹⁰. An often-important role is played by bacteria residing on sinking particles, which convert the particles’ organic carbon into biomass or recycle it back into the dissolved phase^{6,7}. From the perspective of bacteria, the phases of particle decomposition proceed through colonization^{11–13}, enzymatic degradation and the associated consumption of breakdown products to fuel cell growth¹², and finally detachment in pursuit of new particles^{13–15}. Particles are hotspots of enzymatic hydrolysis, where hydrolysis rates greatly exceed those in the surrounding seawater^{6,16}. As a result, most particulate organic carbon (POC) that escapes consumption and modification by higher trophic levels¹⁷ is remineralized to CO₂ by microbial respiration in the upper water column^{18–20}, so that only 5–25% of the fixed carbon leaves the euphotic zone and only about 1% reaches the sediments, where it remains buried for thousands of years^{18,21,22}. Thus, the degradation of organic particles by bacteria governs a major component of the global carbon cycle⁶, and understanding it is essential to predicting the role of the oceans in regulating atmospheric carbon dioxide.

At the heart of the carbon pump lay two opposing processes: sinking and degradation. Higher sinking speeds enhance the vertical carbon flux by accelerating the descent of particles, whereas deg-

radation reduces the vertical carbon flux by removing carbon from sinking particles. This competition is captured in some models of the Martin curve, the empirical relation describing the decrease in vertical POC flux with depth^{18,23–25}. In such models, the vertical POC flux $F(Z)$ at depth Z is described either by Martin’s classic power-law equation, $F(Z) = F(Z_0)(Z/Z_0)^{-b}$, or by its exponential variant, $F(Z) = F(Z_0)e^{-\lambda(Z-Z_0)/W}$, where Z_0 is the depth of the euphotic layer^{18,23,24}. In the first equation, b is the coefficient of flux attenuation (the higher the value of b , the less carbon reaches the ocean depths). In the second equation, λ is the typical rate of POC degradation and W is the typical sinking speed: their ratio, $Z = W/\lambda$, is the remineralization length scale^{18,23,25}. Studies that modelled the flux decay, for example, by taking into account the contribution of the oceanic food web, the role of mineral ballast in particles or the dependence of bacterial degradation rates on the size of individual particles, have greatly expanded our understanding of the processes driving the biological pump^{2,23,26,27}. Notably, a paradigm underlying all these models is that sinking speed and degradation rate are considered to be independent of each other.

Here we show that sinking speed and degradation rate of particles can in fact be coupled. We demonstrate and quantify this coupling with a series of experiments in which we track the degradation of individual particles. We find that particle degradation rate, measured in the lab, increases with increasing sinking speed up to a speed of 8 m day⁻¹, and saturates for larger sinking speeds at a value that is 12- to 15-fold higher than the degradation rate in the absence of sinking. Using a mathematical model of the vertical carbon flux that accounts for the observed sinking-enhanced degradation, we predict that the enhancement of particle degradation due to sinking can reduce the transport efficiency of the carbon pump by up to two-fold compared with a null model that ignores this enhancement.

¹Institute of Environmental Engineering, Department of Civil, Environmental and Geomatic Engineering, ETH Zurich, Zurich, Switzerland. ²Science for Life Laboratory, Department of Environmental Toxicology, Uppsala University, Uppsala, Sweden. ✉e-mail: alcolombri@ifu.baug.ethz.ch; romanstocker@ethz.ch

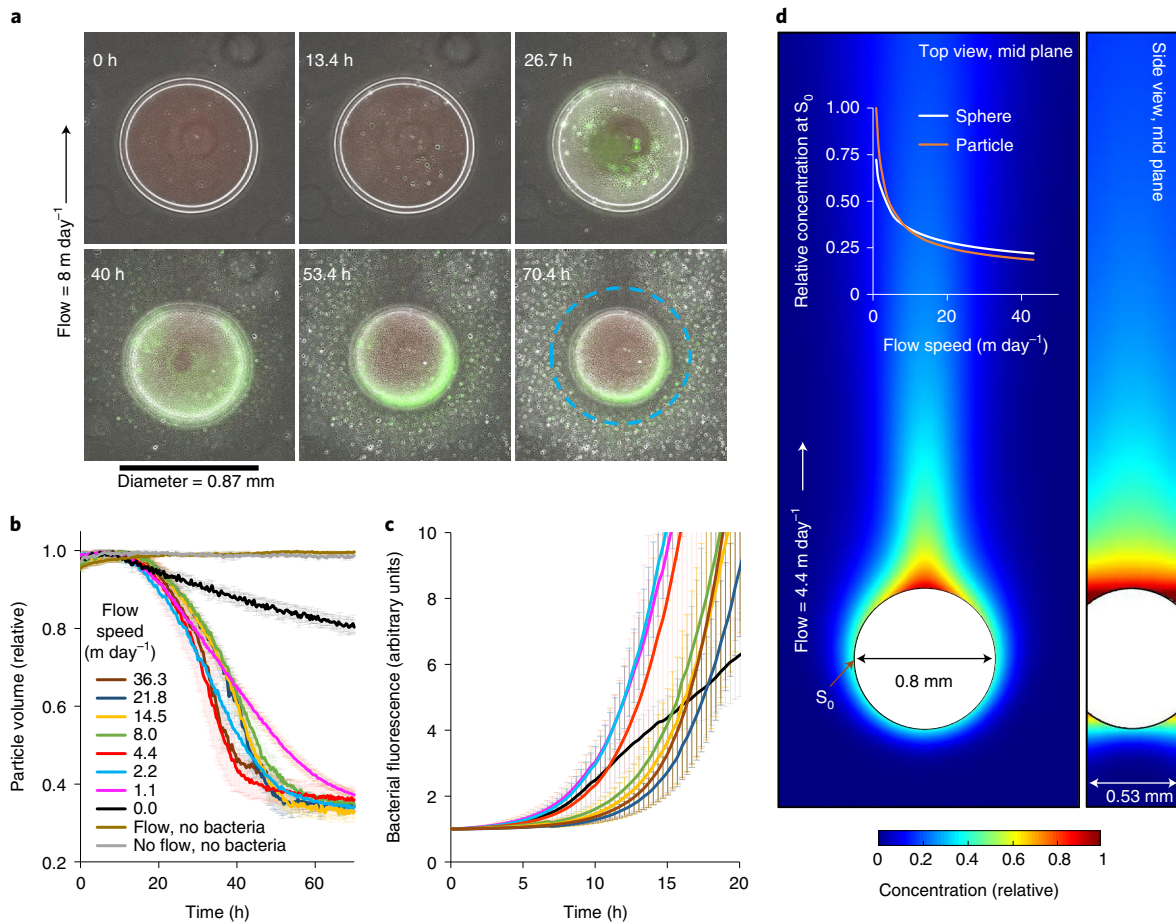


Fig. 1 | Marine particle degradation is flow dependent. **a**, Time-lapse images of alginate particles degraded by *V. cyclitrophicus* ZF270 in flow. Phase images (greyscale) shown with overlaid GFP signal from the bacteria (green). Initial particle diameter (here 0.87 mm) is shown in blue in the final image. **b**, Time series of particle volume during bacterial degradation, relative to initial volume, for different flow speeds (mean (lines) and standard deviation (s.d.; error bars); $n=3$ replicate experiments for each flow speed, except for 4.4 m day⁻¹ for which $n=6$). The flow speed in the absence of bacteria (pale brown line) was 7.25 m day⁻¹. **c**, Time series of bacterial abundance on particles up to 20 h, relative to initial value, for different flow speeds, measured as the average GFP fluorescence intensity at the interface between the particle and the glass slide (Supplementary Video 2). For full 70-hour time series, see Extended Data Fig. 1a. Mean (lines) and s.d. (error bars), colours and n as in **b**. **d**, Nutrient concentration around a particle within the microfluidic channel, as predicted by a mathematical model (top and side views). Nutrient flux from the particle was assumed steady and uniform over the particle surface. Inset: nutrient concentration at the particle's equator (position S_0) as a function of flow speed (orange curve). Results from a model for a freely sinking, 0.8-mm-diameter spherical particle are shown for comparison (white curve).

Sinking enhances the bacterial degradation of particles

To quantify the degradation of sinking particles, we imaged individual alginate particles (diameter 0.88 ± 0.03 mm) pre-colonized by the green fluorescent protein (GFP)-labelled marine gammaproteobacterium *Vibrio cyclitrophicus* ZF270 in a custom microfluidic channel and measured by image analysis their size over time upon exposure to a constant rate of flow (Fig. 1a–c, Supplementary Video 1 and Supplementary Tables 1 and 2 for bacterial characterization). Alginate is a polysaccharide produced by brown macroalgae, particularly in coastal oceans and the Sargasso Sea²⁸, and serves as a carbon source for *V. cyclitrophicus* ZF270 as well as for many other copiotrophic bacteria²⁹. *V. cyclitrophicus* ZF270 is a copiotrophic marine bacterium isolated from large organic particles³⁰, which in our experiments resided on the outer surface of the alginate particles and degraded these using a non-secreted form of alginate lyase (Supplementary Text). Flow with a constant speed towards a fixed particle is equivalent to a particle sinking at that speed in otherwise quiescent fluid. Results from a mathematical model of the transport within our microfluidic device show that the concentration around the particle of leaching nutrient produced by degradation is similar

to that occurring around a freely sinking particle³¹, indicating that our model system captures the fundamental role of sinking on transport (Fig. 1d; Supplementary Text).

Particle degradation in the presence of flow differed dramatically from degradation without flow (compare Supplementary Video 1a,b). For flow speeds corresponding to natural sinking speeds of marine snow³², the volume of individual particles exhibited sigmoidal dynamics over time, with a lag time of 10–20 hours followed by rapid shrinking lasting 15–40 hours (Fig. 1a,b). Particles remained nearly round while shrinking and bacteria were confined to the particle surface, without infiltrating it (Fig. 1a and Supplementary Video 1), so that the reduction in particle volume is a good proxy for particle degradation (Supplementary Text and Extended Data Fig. 1). Particle degradation was accompanied by exponential cell growth fuelled by the breakdown products, as revealed by the dynamics of bacterial GFP fluorescence on the particle (Fig. 1c and Supplementary Video 2). The maximum degradation rate occurred after 30–40 hours (depending on the flow rate), after the particle surface became entirely covered by bacteria (Fig. 1b and Supplementary Video 1). The process ended with the detachment

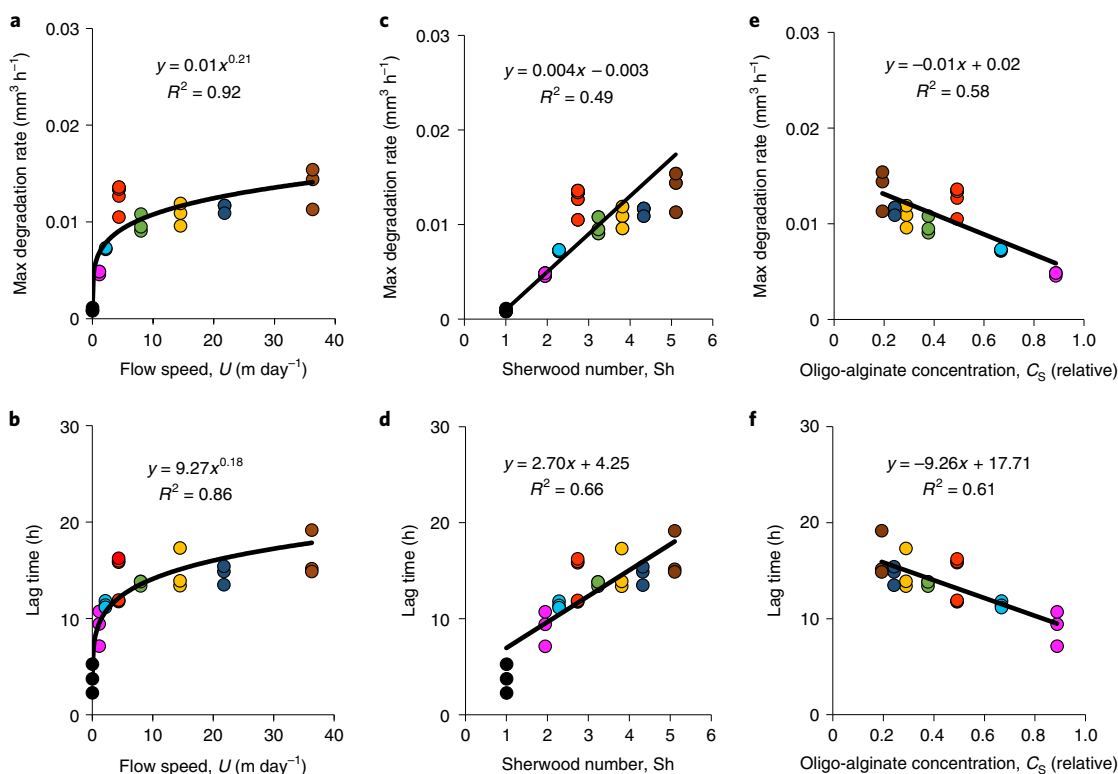


Fig. 2 | Flow plays a key role in determining bacterial growth on, and degradation of, model marine particles. a–f, Maximum degradation rate of alginate particles (**a,c,e**) and lag time of bacteria growing on particles (**b,d,f**), as a function of flow speed, U (**a,b**), Sherwood number, Sh (**c,d**) and oligo-alginate concentration on the particle surface, C_s (**e,f**) (see the ‘COMSOL transport model’ section in the Methods). Curves show power-law (**a,b**) or linear least-squares (**c–f**) fits to the data (R^2 shown in panels, $P < 0.0001$ in all cases). The linear fit in **c** was constrained to intersect with the rate of degradation ($1 \times 10^{-3} \text{ mm}^3 \text{ h}^{-1}$) obtained at no-flow ($Sh = 1$). In all panels, colour code for flow speeds as in Fig. 1b.

of a majority of the bacteria, leaving a fraction (32–37% by volume) of the particle unconsumed, even after 70 hours (Supplementary Video 2 and Fig. 1a,b).

In contrast, the experiments without flow showed much slower degradation dynamics and a linear rather than sigmoidal decrease in particle volume, accompanied by bacterial growth that had a short lag and was linear with time (Fig. 1b,c and Supplementary Videos 1a and 2). Fluid flow was previously shown to counteract O_2 limitation within marine particles³³. However, the difference we observed between degradation rates under flow and no-flow conditions was not a consequence of O_2 limitation under no-flow conditions, for even without flow, the diffusive flux of O_2 into the device was sufficient to support the bacterial population on the particle (Supplementary Text, Supplementary Videos 1 and 2 and Extended Data Fig. 1b).

Controlling sinking speed by imposing a given flow rate in our experiments allowed us to isolate the effect of flow on the dynamics of particle degradation and bacterial growth. With increasing flow speed, the maximum degradation rate increased as a power law with exponent 0.21 (Fig. 2a). Bacterial growth dynamics were also flow-dependent: higher flow rates caused longer lag times in growth, yielding a power-law dependence of lag time on flow rate with exponent 0.18 (Fig. 2b). Both maximum degradation rate and lag time showed a linear correlation ($R^2 = 0.49$ and 0.66, respectively) with the Sherwood number, Sh , the dimensionless parameter quantifying the ratio of total (that is, advective plus diffusive) mass transfer to/from the particle to diffusive mass transfer alone (Fig. 2c,d)³⁴. This signifies that the transport of nutrients by fluid flow plays an important role in setting the degradation rate.

The role of flow is also evidenced by the negative linear correlation of both the maximum degradation rate and the bacterial lag

time ($R^2 = 0.58$ and 0.61, respectively) with the concentration on the surface of the particle of oligo-alginate, the byproduct of the enzymatic degradation of alginate, predicted from our transport model (Figs. 1d and 2e,f). These negative correlations suggest that the rate of particle degradation is regulated by the concentration of the byproduct oligo-alginate within the boundary layer, which in turn is directly affected by fluid flow (Fig. 1d). This hypothesis is also supported by Raman microspectroscopy measurements of the microenvironment surrounding particles, which revealed an accumulation of oligo-alginate on the surface of the particle even at intermediate flow speeds during bacterial degradation, consumption and growth (Extended Data Fig. 2; Methods).

Oligomers inhibit the enzymatic degradation of particles

We hypothesised that the bacterial alginate-lyase enzymes responsible for particle degradation are inhibited by high concentrations of dissolved oligo-alginate. This hypothesis was supported by the results of three experiments. First, we quantified the degradation of particles in the presence of flow of solutions containing different concentrations of oligo-alginate. The addition of oligo-alginate reduced the rate of particle degradation by bacteria by up to 11-fold, in a concentration-dependent manner (Fig. 3a,b and Supplementary Video 3). This effect arose independently of effects on bacterial population growth on the particle, which in fact increased at high oligo-alginate concentration (Extended Data Fig. 3 and Supplementary Video 3). Second, we quantified the degradation of particles in the presence of rich medium in the flow (1% marine broth 2216), instead of oligo-alginate. The addition of rich medium also increased bacterial growth on the particles, but did not reduce the particle degradation rate, indicating that the reduction

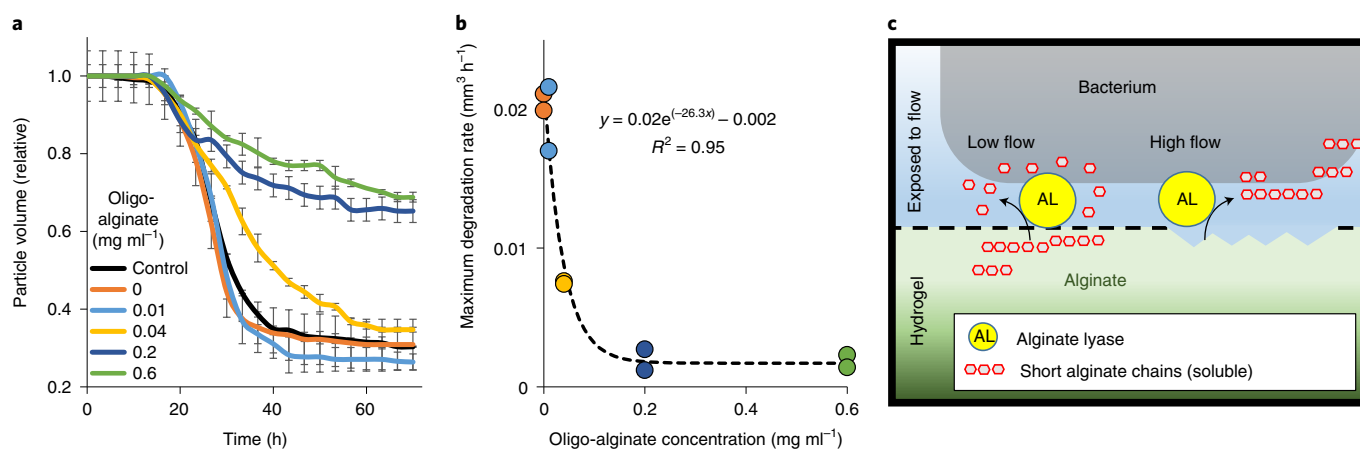


Fig. 3 | High concentrations of oligo-alginate inhibit the degradation of alginate particles. **a**, Time series of particle volume, normalized by initial value, during bacterial degradation under a flow of 7.25 m day⁻¹ of medium supplemented with different concentrations of oligo-alginate (in mg ml⁻¹; colours) or with 1% marine broth 2216 (MB) (black; complementary control). The mean (lines) and s.d. (error bars) ($n = 2$) are shown. **b**, Maximum particle degradation rate as a function of oligo-alginate concentration in the medium (colours as in **a**; $n = 2$). A first-order decay model (dashed line) was fitted to the data. Maximum degradation rate for medium supplemented with 1% marine broth 2216 (MB) was 0.017 ± 0.001 mm³ h⁻¹. **c**, Schematic model of alginate degradation and how it is influenced by flow. Upon colonization, *V. cyclitrophicus* ZF270 expresses alginate lyase (AL) to solubilize, transport and feed on the polysaccharide particle. Under low flow rates (left), the degradation and dissolution of the alginate polysaccharide is inhibited because a high concentration of oligo-alginate accumulates around the particle. The alginate lyase can react with any of the available forms of alginate, but preferentially encounters the dissolved short polymers, oligo-alginate, that have higher concentration and larger diffusivity. High flow removes the short oligo-alginate, removing the competition for enzymatic activity and thereby accelerating depolymerization of the particle (right).

of the degradation rate is specifically caused by oligo-alginate and not by nutrient availability at the particle surface (Fig. 3 and Extended Data Fig. 3). Third, we directly confirmed that high concentrations of oligo-alginate are sufficient to inhibit the degradation of particles by alginate lyase. Using sterile particles, in which degradation was driven solely by pure alginate-lyase enzyme added to the bacteria-free flowing solution, revealed that here, too, degradation was inhibited by the addition of oligo-alginate (Extended Data Fig. 4a and Supplementary Video 4).

Remarkably, the inhibition of alginate lyase during bacterial degradation did not arise by classical product inhibition, whereby the products of the reaction inhibit the specific activity of the enzyme, as the enzymatic activity (measured with enzymes in solution using a plate reader) was unaffected by the addition of oligo-alginate (Extended Data Fig. 4b). Instead, the mechanism we propose is that enzymatic depolymerization, and thus particle degradation, is reduced by the bacterial alginate-lyase enzymes encountering the oligo-alginate molecules that are the initial product of degradation. As they diffuse from the particle on account of being small and dissolved, the degradation products compete for enzymatic activity with the larger polymer molecules that constitute the particle itself. The enhanced degradation in flow thus arises because the otherwise competing oligo-alginate is swept away (Fig. 3c).

Predicted impact on vertical POC flux

To predict the implications of this enhancement of particle degradation by flow and thus the potential impact of coupling between sinking speed and degradation rate on the vertical flux of POC in the ocean, we developed a mathematical model that accounts for the observed coupling (Supplementary Information and Extended Data Figs. 5–9). We consider an initial particle size distribution (PSD) $P(R_0)$ of particles of radius R_0 , with a range of sizes $R_l < R_0 < R_g$ where R_l and R_g are the minimum and maximum initial radius considered respectively, and total concentration of particles C at the euphotic depth Z_0 . Size distributions are chosen based on observed particle distributions in the ocean and account for suspended and sinking POC³⁵. The model evolves the depth $Z(t)$ and radius $R(t)$ of each

particle with time t , based on classic assumptions (including the decreasing sinking speed and increasing density as particle size gets smaller, both based on empirical power laws³⁶) and on our observed dependence of degradation rate on sinking speed (Supplementary Information). Whereas in general, multiple processes affect particle degradation and thus vertical carbon flux, including fragmentation, coagulation or consumption by zooplankton, the model focuses on the contribution of bacterial degradation (it does, however, account for variation in PSDs, and thereby indirectly for the results of particle fragmentation and coagulation; see below). This model, therefore, is not intended to replace large-scale biogeochemical models, but only to provide a measure of the importance of including the mechanism we report. For this reason, we do not attempt to predict the absolute carbon flux at a given location or time. Instead, we predict the vertical carbon flux over depth relative to the flux at the bottom of the euphotic zone, $F(Z)/F(Z_0)$, and compare this with the reference case (null model) in which the effect of flow on degradation is ignored.

Accounting for the observed effect of sinking resulted in a much stronger attenuation of carbon flux with depth, as sinking-enhanced degradation causes more carbon to be remineralized by bacteria in the upper water column. This was reflected in a 2.8-fold higher coefficient of carbon attenuation b in the best-fit Martin curve and in a much shallower half-decay depth of 150 m below Z_0 , compared with ~1450 m in the case without coupling between sinking and degradation (Fig. 4, Supplementary Information). In line with this result, the relative POC transfer efficiency 100 m below the euphotic zone^{2,37}, denoted T_{100} , was 56%, compared with 94% in the case without coupling (Fig. 4, Supplementary Information). Our model thus predicts a large effect, overlooked in current biogeochemical models, of the coupling between sinking and bacterial degradation, which in several regions of the ocean may make an important contribution to setting the vertical flux of carbon (further analysis in Supplementary Information, Extended Data Figs. 5–9).

The impact of the coupling between sinking and degradation is predicted to vary by oceanic province (Supplementary Discussion). To study the potential contribution in different oceanic regions and

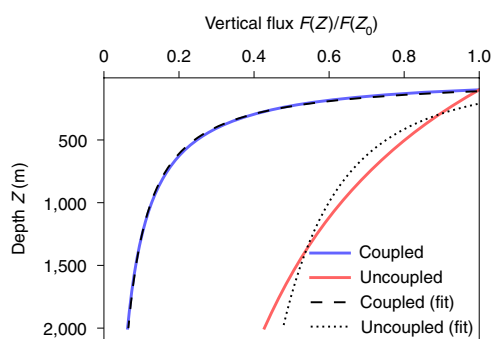


Fig. 4 | The coupling of sinking and degradation can have a major effect on vertical flux of POC in the ocean. Shown is the vertical flux of POC as a function of depth, $F(Z)$, normalized by its initial value $F(Z_0)$ at the euphotic layer depth, $Z_0 = 100$ m, predicted by a model that accounts for the observed coupling of sinking and degradation (blue curve). Also shown is a null model ignoring the coupling, with degradation rate equal to that observed at no flow (red curve). In both models, total particle concentration was 200 per litre, with a power-law size distribution with exponent -4 over particle radii from $R_l = 125 \mu\text{m}$ to $R_g = 750 \mu\text{m}$. Black lines show best fits of a Martin curve $F(Z) = F(Z_0)(Z/Z_0)^{-b}$ to the model predictions, resulting in $b = 0.94$ ($R^2 > 0.99$) for the coupled case (dashed line; of the same order as values obtained from environmental data^{18,44}) and $b = 0.33$ ($R^2 = 0.93$) for the uncoupled case (dotted line). For other model assumptions and additional cases, see the Supplementary Information and Extended Data Figs. 5–9.

in the context of additional processes affecting the biological pump, we quantified T_{100} for different initial particle size distributions (PSDs) in the surface ocean. Steeper PSDs are typical of oligotrophic waters; shallower PSDs are typical of more eutrophic waters^{38,39}. Model results indicate that the coupling of particle degradation and sinking speed strongly enhances particle degradation in eutrophic waters (compared with a model that ignores the coupling), where the relative abundance of larger and thus typically faster sinking particles is greater ($T_{100} = 43\%$ for the coupled case versus $T_{100} = 92\%$ for the uncoupled case, for a PSD with exponent of -2 , corresponding to a 2.14-fold decrease; Supplementary Discussion and Extended Data Fig. 7). We expect this scenario to apply in eutrophic waters, under bloom conditions with strong coagulation of particles and, for example, in the subtropical ocean during winter, where fast sinking particles ($>10 \text{ m day}^{-1}$) contribute considerably to the carbon flux^{2,38,40–42}. A weaker but still considerable effect is observed in oligotrophic waters ($T_{100} = 60\%$ for the coupled case versus $T_{100} = 95\%$ for the uncoupled case, for a PSD with exponent of -5 , corresponding to a 1.58-fold decrease), where the relative abundance of smaller and thus typically slower sinking particles is greater^{2,38,41–43}. We expect this scenario to apply in waters rich with fragmented particles⁹ and, for example, in the subtropical oligotrophic Atlantic and Pacific oceans, the Subarctic Ocean, the North Pacific Ocean and the north-west Mediterranean Sea in the summer, where slow sinking particles ($<10 \text{ m day}^{-1}$) contribute substantially to the carbon flux^{40,41}.

Model results show that the effect of the sinking–degradation coupling is robust to the incorporation of other characteristics of the particle transport process. Accounting for the decrease of enzymatic activity with decreasing temperature, and thus with increasing depth (with a temperature coefficient Q_{10} of 2.5; Supplementary Information), generally increases the transfer efficiency of POC, yet the difference between the coupled and uncoupled cases is preserved ($T_{100} = 74\%$ and $T_{100} = 98\%$, respectively; Supplementary Information and Extended Data Fig. 8). Moreover, the effect of the coupling between sinking and degradation in decreasing the transfer efficiency T_{100} is greater than the effect of temperature

on the degradation rate (Supplementary Discussion). Finally, the temperature-dependence of seawater viscosity has a negligible effect on our predictions of T_{100} (Supplementary Information and Extended Data Fig. 9). In summary, even when taking into account further aspects of the complexity of the natural process, the sinking-enhanced degradation mechanism is predicted to play an important role in setting the bacterial degradation rate of particles in the ocean (Supplementary Discussion).

Although our model results demonstrate that sinking-enhanced degradation, if validated in the environment, can impose an important control on carbon flux, the actual flux at a given location will be further affected by several other factors, including particle consumption by zooplankton¹⁷, particle fragmentation⁹ and local temperature⁴⁴. Indeed, a limitation of our model is that it does not account for processes that may act in concert with sinking-enhanced degradation, such as aggregation/disaggregation and the incorporation of ballast in particles²³, known to affect carbon flux in the ocean. In the environment, particles of a given size can have different sinking speeds, permeabilities and porosities. For example, the inclusion of ballast material, which is dense and non-permeable, may cause the sinking speed to increase as the (often less dense) labile material is degraded: particles may then escape the inhibited degradation experienced at low sinking speeds and operate within a regime of rapid sinking and enhanced degradation. Additionally, aggregation or disaggregation may respectively accelerate or slow down the sinking of particles and thus alter their degradation via the coupling to flow; the actual quantitative importance of these factors will be best quantified using global POC models. These limitations notwithstanding, our work suggests that global models should account for the dependence of degradation rate on sinking speed, provides a quantitative formulation for this dependence and cautions against parameterizing models using degradation rates obtained from quiescent, in vitro experiments, which will considerably underestimate particle degradation rates.

The fundamental transport-based nature of the role of flow suggests that the coupling between sinking and degradation that we reported is not specific to our particular experimental system. The proposed sinking-enhanced degradation mechanism is likely to be independent of the specific bacterial strain causing degradation, for it is apparent when degradation is produced purely by enzymes in solution (Extended Data Fig. 4a and Supplementary Video 4). Support for this generality comes also from additional observations that the same mechanism applies for other polymers found in marine particles: a sinking speed of 7.25 m day^{-1} enhanced degradation by 4.5-fold for chitin particles and by 2.5-fold for short-chain chitosan particles compared with no-flow conditions, for a co-culture of *Vibrio splendidus* 1A01 and *Psychromonas* C606 (Extended Data Fig. 10 and Supplementary Video 5; Methods).

While polymeric carbohydrates such as alginate account for a major fraction of labile carbon in several oceanic regions^{45,46}, often serving as the glue that holds particles together⁴⁷, natural particles harbour greater complexity than our model particles. Thus, further analysis will be required to assess the contribution to particle degradation of chemical composition, as well as other factors such as porosity (which adds degradation from within the particles) and microbial community composition (Supplementary Discussion). The flow due to sinking will also have additional effects that can further affect degradation, such as increasing particle encounters with bacteria¹⁵, decreasing the competitive advantage of non-degrading microbes on particles⁴⁸, and enhancing the flux of oxygen to the interior of particles³³ and of secreted enzymes and signalling molecules away from particles. The formation of a thick biofilm could also change the transport and degradation dynamics⁴⁸. These additional effects notwithstanding, our observations establish the coupling between sinking and degradation as a fundamental mechanism that, together and possibly in synergy with other processes,

can impact the vertical flux of carbon in the ocean. Ultimately, our work shows that not only the ecological interactions on particles⁴⁹ but also the microscale transport dynamics play a fundamental role in determining the degradation rate of particles by bacteria and can contribute to the global-scale carbon flux to the oceans' depths.

Online content

Any methods, additional references, Nature Research reporting summaries, source data, extended data, supplementary information, acknowledgements, peer review information; details of author contributions and competing interests; and statements of data and code availability are available at <https://doi.org/10.1038/s41561-021-00817-x>.

Received: 5 April 2020; Accepted: 19 July 2021;

Published online: 23 September 2021

References

- Boyd, P. W., Claustre, H., Levy, M., Siegel, D. A. & Weber, T. Multi-faceted particle pumps drive carbon sequestration in the ocean. *Nature* **568**, 327–335 (2019).
- Buesseler, K. O. & Boyd, P. W. Shedding light on processes that control particle export and flux attenuation in the twilight zone of the open ocean. *Limnol. Oceanogr.* **54**, 1210–1232 (2009).
- Eppley, R. W. & Peterson, B. J. Particulate organic matter flux and planktonic new production in the deep ocean. *Nature* **282**, 677–680 (1979).
- Jiao, N. et al. Microbial production of recalcitrant dissolved organic matter: long-term carbon storage in the global ocean. *Nat. Rev. Microbiol.* **8**, 593–599 (2010).
- Volk, T., Hoffert, M. I. in *The Carbon Cycle and Atmospheric CO₂: Natural Variations Archean to Present* Vol. 32 (eds Sundquist, E. T. & Broecker, W. S.) 99–110 (American Geophysical Union, 1985).
- Smith, D. C., Simon, M., Alldredge, A. L. & Azam, F. Intense hydrolytic enzyme activity on marine aggregates and implications for rapid particle dissolution. *Nature* **359**, 139–142 (1992).
- Silver, M. W., Shanks, A. L. & Trent, J. D. Marine snow: microplankton habitat and source of small-scale patchiness in pelagic populations. *Science* **201**, 371–373 (1978).
- Lampitt, R. S., Wishner, K. F., Turley, C. M. & Angel, M. V. Marine snow studies in the Northeast Atlantic Ocean: distribution, composition and role as a food source for migrating plankton. *Mar. Biol.* **116**, 689–702 (1993).
- Briggs, N., Dall'Olmo, G. & Claustre, H. Major role of particle fragmentation in regulating biological sequestration of CO₂ by the oceans. *Science* **367**, 791–793 (2020).
- Giering, S. L. C. et al. Reconciliation of the carbon budget in the ocean's twilight zone. *Nature* **507**, 480–483 (2014).
- Smriga, S., Fernandez, V. I., Mitchell, J. G. & Stocker, R. Chemotaxis toward phytoplankton drives organic matter partitioning among marine bacteria. *Proc. Natl Acad. Sci. USA* **113**, 1576–1581 (2016).
- Biddanda, B. Microbial aggregation and degradation of phytoplankton-derived detritus in seawater. II. Microbial metabolism. *Mar. Ecol. Prog. Ser.* **42**, 89–95 (1988).
- Kjørboe, T., Grossart, H. P., Ploug, H. & Tang, K. Mechanisms and rates of colonisation of sinking aggregates. *Appl. Environ. Microbiol.* **68**, 3996–4006 (2002).
- Yawata, Y. et al. Competition-dispersal tradeoff ecologically differentiates recently speciated marine bacterioplankton populations. *Proc. Natl Acad. Sci. USA* **111**, 5622–5627 (2014).
- Singh, P. K. et al. *Vibrio cholerae* combines individual and collective sensing to trigger biofilm dispersal. *Curr. Biol.* **27**, 3359–3366.e7 (2017).
- Buchan, A., LeClerc, G. R., Gulvik, C. A., González, J. M. & González, J. M. Master recyclers: features and functions of bacteria associated with phytoplankton blooms. *Nat. Rev. Microbiol.* **12**, 686–698 (2014).
- Ebersbach, F. & Trull, T. W. Sinking particle properties from polyacrylamide gels during the Kerguelen ocean and plateau compared study (KEOPS): zooplankton control of carbon export in an area of persistent natural iron inputs in the Southern Ocean. *Limnol. Oceanogr.* **53**, 212–224 (2008).
- Martin, J. H., Knauer, G. A., Karl, D. M. & Broenkow, W. W. VERTEX: carbon cycling in the Northeast Pacific. *Deep Sea Res. A* **34**, 267–285 (1987).
- Ducklow, H. W., Steinberg, D. K. & Buesseler, K. O. Upper ocean carbon export and the biological pump. *Oceanography* **14**, 50–58 (2001).
- Stukel, M. R., Song, H., Goericke, R. & Miller, A. J. The role of subduction and gravitational sinking in particle export, carbon sequestration, and the remineralization length scale in the California Current ecosystem. *Limnol. Oceanogr.* **63**, 363–383 (2018).
- Siegel, D. A. et al. Prediction of the export and fate of global ocean net primary production: the exports science plan. *Front. Mar. Sci.* **3**, 22 (2016).
- Dunne, J. P., Sarmiento, J. L. & Gnanadesikan, A. A synthesis of global particle export from the surface ocean and cycling through the ocean interior and on the seafloor. *Global Biogeochem. Cycles* **21**, GB4006 (2007).
- Armstrong, R. A., Lee, C., Hedges, J. I., Honjo, S. & Wakeham, S. G. A new, mechanistic model for organic carbon fluxes in the ocean based on the quantitative association of POC with ballast minerals. *Deep Sea Res. II* **49**, 219–236 (2001).
- Lutz, M., Dunbar, R. & Caldeira, K. Regional variability in the vertical flux of particulate organic carbon in the ocean interior. *Global Biogeochem. Cycles* **16**, 11–11–18 (2002).
- Williams, R. G. & Follows, M. J. *Ocean Dynamics and the Carbon Cycle: Principles and Mechanisms* (Cambridge Univ. Press, 2011).
- Omand, M. M., Govindarajan, R., He, J. & Mahadevan, A. Sinking flux of particulate organic matter in the oceans: sensitivity to particle characteristics. *Sci. Rep.* **10**, 5582 (2020).
- Henson, S. A., Sanders, R. & Madsen, E. Global patterns in efficiency of particulate organic carbon export and transfer to the deep ocean. *Global Biogeochem. Cycles* **26**, GB1028 (2012).
- Krause-Jensen, D. & Duarte, C. M. Substantial role of macroalgae in marine carbon sequestration. *Nat. Geosci.* **9**, 737–742 (2016).
- Hehemann, J. H. et al. Adaptive radiation by waves of gene transfer leads to fine-scale resource partitioning in marine microbes. *Nat. Commun.* **7**, 12860 (2016).
- Hunt, D. E. et al. Resource partitioning and sympatric differentiation among closely related bacterioplankton. *Science* **320**, 1081–1085 (2008).
- Kjørboe, T. & Jackson, G. A. Marine snow, organic solute plumes, and optimal chemosensory behavior of bacteria. *Limnol. Oceanogr.* **46**, 1309–1318 (2001).
- Laurenceau-Cornec, E. C., Trull, T. W., Davies, D. M., De La Rocha, C. L. & Blain, S. Phytoplankton morphology controls on marine snow sinking velocity. *Mar. Ecol. Prog. Ser.* **520**, 35–56 (2015).
- Ploug, H. & Grossart, H. P. Bacterial production and respiration in suspended aggregates—a matter of the incubation method. *Aquat. Microb. Ecol.* **20**, 321–329 (1999).
- Karp-Boss, L., Boss, E. & Jumars, P. A. Nutrient fluxes to planktonic osmotrophs in the presence of fluid motion. *Oceanogr. Mar. Biol.* **34**, 71–107 (1996).
- Guidi, L. et al. Plankton networks driving carbon export in the oligotrophic ocean. *Nature* **532**, 465–470 (2016).
- Allredge, A. L. & Gotschalk, C. In situ settling behavior of marine snow. *Limnol. Oceanogr.* **33**, 339–35 (1988).
- Buesseler, K. O., Boyd, P. W., Black, E. E. & Siegel, D. A. Metrics that matter for assessing the ocean biological carbon pump. *Proc. Natl Acad. Sci. USA* **117**, 9679–9687 (2020).
- Guidi, L. et al. Effects of phytoplankton community on production, size and export of large aggregates: a world-ocean analysis. *Limnol. Oceanogr.* **54**, 1951–1963 (2009).
- Stemmann, L. & Boss, E. Plankton and particle size and packaging: from determining optical properties to driving the biological pump. *Ann. Rev. Mar. Sci.* **4**, 263–290 (2012).
- Trull, T. W. et al. In situ measurement of mesopelagic particle sinking rates and the control of carbon transfer to the ocean interior during the Vertical Flux in the Global Ocean (VERTIGO) voyages in the North Pacific. *Deep Sea Res. II* **55**, 1684–1695 (2008).
- Alonso-Gonzalez, I. J. et al. Role of slowly settling particles in the ocean carbon cycle. *Geophys. Res. Lett.* **37**, L13608 (2010).
- Jokulsdottir, T. & Archer, D. A stochastic, Lagrangian model of sinking biogenic aggregates in the ocean (SLAMS 1.0): model formulation, validation and sensitivity. *Geosci. Model Dev.* **9**, 1455–1476 (2016).
- Herndl, G. J. & Reinthaler, T. Microbial control of the dark end of the biological pump. *Nat. Geosci.* **6**, 718–724 (2013).
- Marsay, C. M. et al. Attenuation of sinking particulate organic carbon flux through the mesopelagic ocean. *Proc. Natl Acad. Sci. USA* **112**, 1089–1094 (2015).
- Kim, B. K. et al. Vertical distributions of macromolecular composition of particulate organic matter in the water column of the Amundsen Sea polynya during the summer in 2014. *J. Geophys. Res. Oceans* **123**, 1393–1405 (2018).
- Becker, S. et al. Laminarin is a major molecule in the marine carbon cycle. *Proc. Natl Acad. Sci. USA* **117**, 6599–6607 (2020).
- Allredge, A. L., Passow, U. & Logan, B. E. The abundance and significance of a class of large, transparent organic particles in the ocean. *Deep Sea Res. I* **40**, 1131–1140 (1993).
- Drescher, K., Nadell, C. D., Stone, H. A., Wingreen, N. S. & Bassler, B. L. Solutions to the public goods dilemma in bacterial biofilms. *Curr. Biol.* **24**, 50–55 (2014).
- Datta, M. S. et al. Successions on model marine particles. *Nat. Commun.* **7**, 11965 (2016).

Publisher's note Springer Nature remains neutral with regard to jurisdictional claims in published maps and institutional affiliations.

© The Author(s), under exclusive licence to Springer Nature Limited 2021

Methods

Bacterial culture. *V. cyclitrophicus* ZF270, kindly provided by M. Polz (Massachusetts Institute of Technology), was originally isolated from the coast of New England, United States. A GFP-labelled strain was obtained from previous work¹⁴. All experiments were performed in *f/2* medium, with artificial seawater, the exclusion of sodium metasilicate and the addition of 1 mM NH₄Cl₂ (–Si +NH₄) (NCMA Bigelow Laboratory for Ocean Sciences). Artificial seawater was prepared by dissolving 35 g of sea salt (Instant Ocean, Spectrum Brands) in 1 l double distilled water (DDW), filtering through a 0.2 μm filter and autoclaving. For the preparation of alginate plates, a solution of *f/2* (–Si +NH₄) medium was mixed with 1% weight per volume (w/v) Bacto Agar (Becton Dickinson) and 0.5% (w/v) alginic acid sodium salt from brown algae (medium viscosity, Sigma-Aldrich) and sterilized by autoclave. For general bacterial culture, 10% marine broth 2216 (Becton Dickinson) in artificial seawater was used. Plasmid selection during growth was performed using spectinomycin (50 μg ml^{–1}; Sigma-Aldrich).

Particle preparation. Alginate particles were prepared using a mix of alginic acid sodium salt from brown algae (medium viscosity, Sigma-Aldrich) and alginate labelled with rhodamine (0.015% w/v, medium viscosity; Creative PEGWorks). To solubilize the alginate, 50 mM EDTA, pH = 8.0, in DDW was added. To form particles, the alginate solution was dripped from a 1 ml syringe with a needle, at a rate of 60 μl min^{–1}, from a height of 20 cm above a beaker containing 0.5 M CaCl₂ in DDW. The CaCl₂ solution was stirred constantly using a magnetic stir-bar (300 rpm). Drop size was optimized by blowing nitrogen flux (50–300 mbar) from a distance of 2 cm from the tip of the alginate source. Particle sizes were measured under a microscope and the nitrogen flux was optimized to provide particles of diameter 0.88 ± 0.03 mm. The particles were collected from the CaCl₂ solution using a 100-μm filter and kept at 4 °C in fresh 0.5 M CaCl₂ solution until used. Chitin and short-chain chitosan particles were prepared as previously described³⁰. Briefly, chitin from shrimp exoskeletons (Sigma-Aldrich, C7170) was dissolved in *N*-dimethylacetamide with 5% LiCl (w/v) to give 1% (w/v) final concentration. This solution was dripped from a syringe, as described above for the alginate solution, into an absolute ethanol solution to form chitin beads. Short-chain chitosan particles were prepared with the same approach, but with chitin that was treated beforehand for seven days in 10% HCl (v/v) and then one day in 5 M NaOH. Before making the chitosan particles, the solution was repeatedly washed with DDW until a pH of 6.5 was achieved.

Particle degradation in a microfluidic chip. Prior to experiments, *V. cyclitrophicus* ZF270 were starved for carbon for 2 hours in *f/2* (–Si +NH₄) medium. The particles were taken from the 0.5 M CaCl₂ solution and allowed to equilibrate by incubation in 15 ml *f/2* (–Si +NH₄) medium under slow shaking (60 rpm). Bacterial degradation of alginate particles was studied within a custom-made six-channel microfluidic chip (Sticky-Slide V1 0.4, IBIDI). Six single particles were collected using a pipettor equipped with chopped-edge tips and placed individually in the six channels of the slide. Before experiments were started, the particles were incubated for 60 min with the previously starved *V. cyclitrophicus* (ZF270 GFP-labelled) at final optical density (O.D.) at 600 nm of 0.0025. The sticky-slide channels were closed with a sterilized (ultraviolet (UV)-treated) cover slide to trap one particle at the centre of each channel. Using a syringe, the channel was manually supplied with 0.3 ml of medium to flush out unbound bacteria and to fill the channel with liquid while avoiding trapping bubbles. A syringe pump (Harvard PHD2000) was then used to maintain flow in the channels with *f/2* (–Si +NH₄) medium at the desired rate (1–36.3 m day^{–1}). In the replicates with zero flow, the inlet of the channel was gently blocked with parafilm to allow oxygen permeability but reduce water evaporation. The microfluidic chip was mounted on a microscope for visualization. All experiments were performed at 25 °C. No antibiotic was used for selection on the chip, but no loss of fluorescence was observed during the experiments. Identical experiments were performed using chitin and short-chain chitosan particles, but with a mix of *V. splendidus* (1A01) and *Psychromonas* (6C06) instead of *V. cyclitrophicus* ZF270, and with initial inoculum density of 0.02 O.D. from each strain instead of 0.0025 O.D.

Visualization and image analysis. Experiments were visualized using a Nikon Eclipse TI-2 microscope at magnification ×100, capturing phase and fluorescence images at 20 min intervals for 70 hours using an Orca flash 4.0 (Hamamatsu) camera. Images were analysed using NIS-Elements 4.40.00 (Nikon) and the MATLAB (R2016b) image analysis toolbox. The diameter of each particle was measured using the 'imfindcircles' function in MATLAB, on the images taken from the mid plane of the particle. Bacterial growth was estimated using NIS-Elements based on the average fluorescence intensity obtained from the lowest plan, at the interface between the glass and the alginate particle. The measurement area in all experiments was limited to the particle boundaries and excluded bacterial growth in the surrounding medium. The volume of each particle was estimated using the particle diameter by assuming a perfect spherical shape. Particle volume was normalized to the maximum value and the average fluorescence intensity was normalized to the initial values. All experiments were visualized for 70 hours, except those using a flow rate of 36.3 m day^{–1}, in which the particles were sufficiently degraded and carried away by the fluid flow after ~50 hours.

Oxygen-consumption measurements. Three independent cultures, containing 18 alginate particles in 500 μl of *f/2* (–Si +NH₄) medium, were incubated at 30 °C with 800 rpm shaking in 2 ml Eppendorf tubes. The primary inoculum had O.D. = 0.01 after dilution from a starter culture that was grown in marine broth 2216 for 5 hours to O.D. = 0.15. After 40 hours, the supernatant (which includes the unbound bacteria) was removed and the particle with a small amount of the leftover supernatant was suspended gently in 2 ml of fresh *f/2* (–Si +NH₄) medium. Particles were transferred to 2 ml respiration vials containing an O₂ sensor spot (OXSP5, PyroScience) and the O₂ consumption measured at room temperature over 4 hours. As a control, O₂ consumption was measured for 18 particles with no bacteria. The particles and all content were then transferred to an 8-well μ-slide (ibidi) to measure particle diameter by microscopy. To count cell number, the particles were dissolved using 100 μl of 0.5 M EDTA. The dissolved particles were vortexed until fully dissolved to suspend all the previously attached bacteria. The dissolved particle solution was stained with SYBR green (1:100 from stock solution) and diluted 1:10 with artificial seawater, then cells were counted by flow cytometry (CytoFLEX, Beckman Coulter) with flow rate of 30 μl min^{–1}.

Oxygen flux to the particle. O₂ diffusive flux to the particle (in the absence of flow) was estimated using the equation for mass transfer to a perfectly absorbing sphere

$$Q = 4\pi D r C,$$

where Q is the flux (mol min^{–1}), D is the diffusion coefficient of O₂ in water (2 × 10^{–5} cm² s^{–1}) at a temperature of 25 °C, r is the radius of the sphere (0.05 cm) and C is the concentration of dissolved oxygen in seawater at a temperature of 25 °C (0.2 μmol cm^{–3}). Using these values, we obtain an estimated flux of 151 pmol min^{–1}. Note that this simplified calculation only provides an approximate estimate of the diffusion flux within the chamber; however, when compared with the estimated oxygen requirements of bacteria on the particle it suggests that even in the absence of flow, the O₂ flux is about 17-fold higher than the consumption rate and thus O₂ flux is unlikely to limit degradation rates (the estimated O₂ requirement per particle is 8.9 ± 0.7 pmol min^{–1} per particle, at peak growth, 40 h post inoculation, $n = 3$).

COMSOL transport model. For the model of nutrient transport in flow around our particles, we used the COMSOL Multiphysics (5.5) software to solve the coupled physics problem of transport of dilute species together with laminar flow in the chamber. In the simulation, a 0.8 mm sphere was placed in the centre of a 5 mm × 20 mm × 0.53 mm channel. The sphere is taller than the channel, thus creating a 'pita'-like structure that resembles the squeezed alginate particle. A steady surface flux equal to 3.5 × 10^{–6} mol m^{–2} s^{–1} was used to mimic the leakage of oligo-alginate from the particle. The diffusion coefficient of the oligo-alginate was set to 1 × 10^{–9} m² s^{–1}. The concentration of the solute was computed on the side of the particle surface as a function of the flow rate (Fig. 1d). For comparison, we solved a transport model for a simple sphere in flow with identical parameters (Fig. 1d). The COMSOL model files can be obtained from Zenodo (<https://doi.org/10.5281/zenodo.4818505>).

Oligo-alginate preparation. Oligo-alginate was prepared by mixing 1% (w/v) alginate (medium viscosity; Sigma-Aldrich) with 20 μg ml^{–1} alginate lyase and 2 mM CaCl₂ in 10 mM MOPS buffer (pH = 7.0). The enzymatic reaction was mixed (600 rpm) overnight at room temperature. The solution was then filter centrifuged (Centricon 10 kDa, Millipore). The flow-through was collected and the salinity adjusted to 35 g l^{–1} with instant ocean solute. The solution was frozen at –20 °C until further use.

Bacterial degradation of particles as a function of oligo-alginate concentration. Incubation of particles in the microfluidic chip and experimental procedures were performed as described above. Flow of 7.25 m day^{–1} was provided for 17 hours until cells entered the exponential growth phase. The medium being flowed into each channel was then changed to a solution containing oligo-alginate (>10 kDa) (either 0.01 mg ml^{–1}, 0.04 mg ml^{–1}, 0.2 mg ml^{–1} or 0.6 mg ml^{–1}), no oligo-alginate or 1% marine broth 2216. The change to the new medium took 20–40 min, during which no flow was applied to any of the channels. Visualization and data analysis were performed as described above.

Enzymatic degradation of particles as a function of oligo-alginate concentration. The particles were trapped in a microfluidic channel as in the other experiments and supplied with medium and alginate-lyase enzyme (10 μg ml^{–1}) at a flow rate of 7.25 m day^{–1}. For comparison, experiments using a similar solution complemented with 1 mg ml^{–1} oligo-alginate and one with no enzyme but with oligo-alginate (1 mg ml^{–1}) were performed in parallel. Degradation was monitored at intervals of 1 min over 180 min by video microscopy and image analysis. Alginate lyase activity was also measured using a plate reader by monitoring the UV absorption at 235 nm as an indication of alginate degradation. The activity was measured in 10 mM MOPS buffer containing 20 μg ml^{–1} alginate lyase, 0.1% (w/v) sodium alginate, 2 mM CaCl₂ and the different concentrations of oligo-alginate (0 mg ml^{–1}, 0.008 mg ml^{–1}, 0.016 mg ml^{–1}, 0.031 mg ml^{–1}, 0.063 mg ml^{–1}, 0.125 mg ml^{–1}, 0.250 mg ml^{–1} and 0.500 mg ml^{–1}).

Raman microspectroscopy to estimate oligo-alginate distribution within and around the particles. A colonized alginate particle was imaged in a microfluidic device (sticky-slide I Luer, ibidi), 42 hours post inoculation using a confocal Raman system under flow of 7.25 m day^{-1} . A confocal Raman microspectroscopy (Horiba LabRAM HR Evolution, Horiba Scientific) was used to take the bright-field image and to measure the Raman scattering signal of the alginate particle. The resulting degraded particle was visualized by stitching the 660 images (22×30), Raman mapped with step size of $20 \mu\text{m}$ (in both x and y directions) in two sessions, 'top' and 'bottom', bottom side mapped second. The Raman laser (532 nm, neodymium-doped yttrium aluminum garnet (Nd:YAG) at 1 W) was focused using a $\times 60$ water-immersion objective (Plan Apo VC $60 \times A/1.2$ WI, Nikon) with pinhole size $200 \mu\text{m}$ and 1 s exposure time was used at each measurement point. As a control, a sterile particle was measured under the same conditions. To evaluate the spatial distribution of the lysed polymer, the carboxyl ion peak (COO^- ; $1390\text{--}1440 \text{ cm}^{-1}$) was mapped. Integrated Raman intensity ($I_{1390\text{--}1440}$) was normalized by the glass peak intensity ($I_{520\text{--}570}$). No smoothing or baseline subtraction were used. The concentration of the carboxyl ion, a proxy for dissolved oligo-alginate released by bacterial degradation, was highest at the particle boundary and decreased towards the particle centre (Extended Data Fig. 2c). In contrast, the spatial distribution of the carboxyl ion was homogeneous in the control sample (Extended Data Fig. 2d).

Modelling the potential effect of sinking-enhanced degradation on the efficiency of the ocean's carbon pump. To investigate how the coupling of the flow caused by sinking and the rate of degradation revealed in our experiments can affect the vertical flux of carbon in the ocean, we developed a model of marine particle degradation and sinking that incorporates the observed effects of flow. Full details can be found in the Supplementary Information. The computer code used for modelling the potential effect of sinking-enhanced degradation on the efficiency of the ocean's carbon pump is available for download from Zenodo (<https://doi.org/10.5281/zenodo.5233234>).

Data availability

The datasets and representative videos generated and analysed during the study are available in the Supplementary Information of the paper. The raw videos generated and analysed during the study are available for download from: <https://doi.org/10.3929/ethz-b-000488179>. Source data are provided with this paper.

Code availability

The computer codes used during the study are available for download from Zenodo (COMSOL transport model, <https://doi.org/10.5281/zenodo.4818505>; model of sinking-enhanced degradation, <https://doi.org/10.5281/zenodo.5233234>).

References

- Muhammad Yusof, N. L. B., Lim, L. Y. & Khor, E. Preparation and characterization of chitin beads as a wound dressing precursor. *J. Biomed. Mater. Res.* **54**, 59–68 (2001).

- McDonnell, A. M. P. & Buessler, K. O. Variability in the average sinking velocity of marine particles. *Limnol. Oceanogr.* **55**, 2085–2096 (2010).
- Enke, T. N., Leventhal, G. E., Metzger, M., Saavedra, J. T. & Cordero, O. X. Microscale ecology regulates particulate organic matter turnover in model marine microbial communities. *Nat. Commun.* **9**, 2743 (2018).
- Ebrahimi, A., Schwartzman, J. & Cordero, O. X. Cooperation and spatial self-organization determine rate and efficiency of particulate organic matter degradation in marine bacteria. *Proc. Natl Acad. Sci. USA* **116**, 23309–23316 (2019).

Acknowledgements

We thank R. Naisbit for help with editing and members of the Simons Foundation PriME collaboration for fruitful discussions. We gratefully acknowledge funding from the European Molecular Biology Organization (EMBO; ALTF 1109-2016) and the Human Frontier Science Program (HFSP; LT001209/2017) to U.A.; the European Union's Horizon 2020 research and innovation programme under a Marie Skłodowska-Curie grant agreement (No. 798411) to F.J.P.; the Science for Life Laboratory (SciLifeLab Fellowship grant, SLL 2019/2) to L.B.; and from a Gordon and Betty Moore Foundation Symbiosis in Aquatic Systems Investigator Award (GBMF9197; <https://doi.org/10.37807/GBMF9197>), the Simons Foundation through the Principles of Microbial Ecosystems (PriME) collaboration (grant 542395) and the Swiss National Science Foundation, National Centre of Competence in Research (NCCR) Microbiomes (No. 51NF40_180575) to R.S.

Author contributions

U.A., F.J.P., V.I.F. and R.S. designed the research. U.A., K.S.L. and L.B. conducted the experiments. U.A. analysed the data. F.J.P., V.I.F. and U.A. developed the theoretical models. F.J.P. performed the numerical simulations. U.A., F.J.P., V.I.F. and R.S. wrote the paper.

Competing interests

The authors declare no competing interests.

Additional information

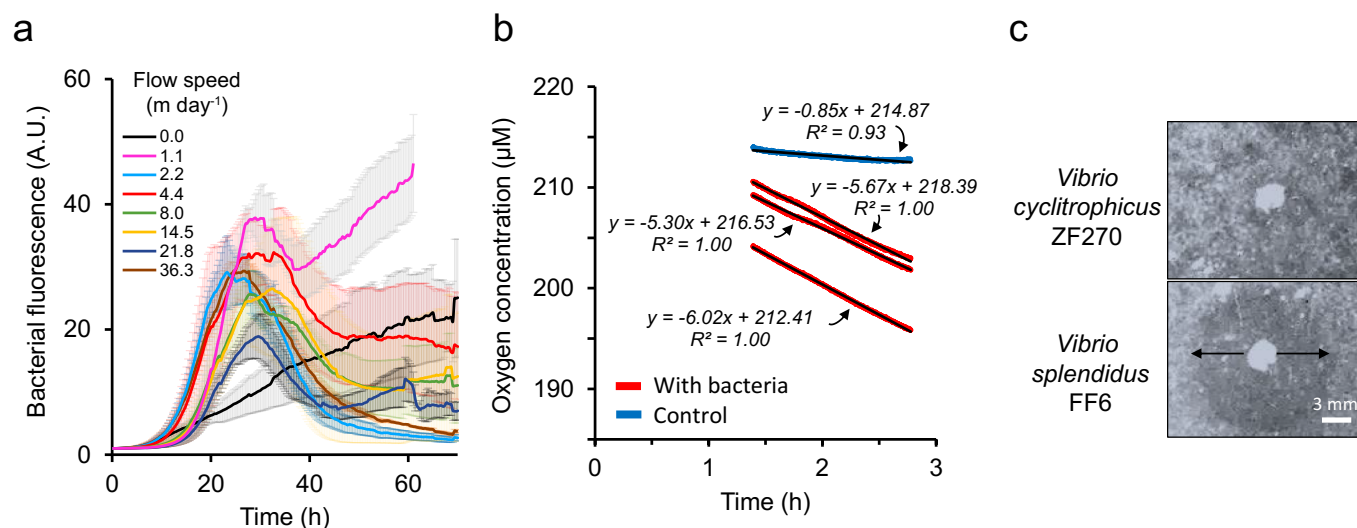
Extended data is available for this paper at <https://doi.org/10.1038/s41561-021-00817-x>.

Supplementary information The online version contains supplementary material available at <https://doi.org/10.1038/s41561-021-00817-x>.

Correspondence and requests for materials should be addressed to Uria Alcolombri or Roman Stocker.

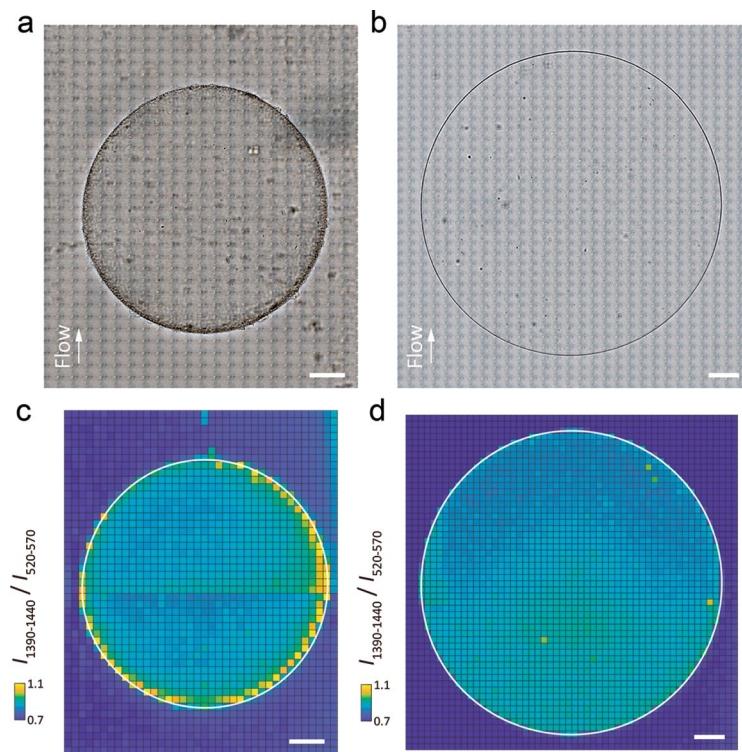
Peer review information *Nature Geoscience* thanks Philip Boyd and the other, anonymous, reviewer(s) for their contribution to the peer review of this work. Primary handling editor: James Super.

Reprints and permissions information is available at www.nature.com/reprints.



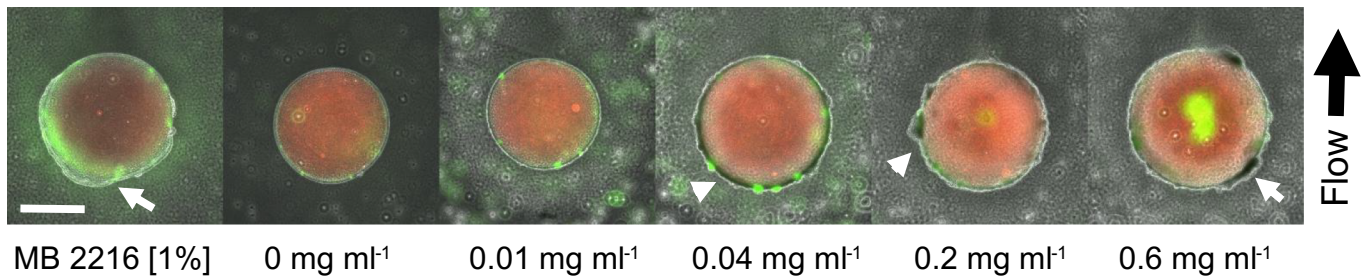
Extended Data Fig. 1 | Growth, respiration and localisation of alginate lyases of *Vibrio cyclitrophicus* ZF270 grown on alginate as a sole carbon source.

(a) Growth of *Vibrio cyclitrophicus* ZF270 on alginate particles under different flow rates. Bacterial growth was quantified as the average GFP fluorescence intensity at the interface between the alginate particle and the glass slide. All data normalized to initial values, error bars are standard deviations of three independent replicates. An expanded view of the exponential phase (0–20 h) is presented in Fig. 1c. A.U. = arbitrary units. **(b)** Respiration rate of *Vibrio cyclitrophicus* ZF270 grown on alginate particles. Respiration was measured in 2 ml vials each containing 18 alginate particles (diameter = 0.80 ± 0.05 mm) pre-colonized with *Vibrio cyclitrophicus* ZF270. O₂ concentration was measured using O₂-sensitive optode sensors and plotted as a function of time for three replicates (see Methods). Values were used to estimate O₂ consumption per particle (8.9 ± 0.7 pmol min⁻¹ particle⁻¹; at peak growth, 40 h post-inoculation, $n = 3$) and per bacterium (0.07 ± 0.02 fmol min⁻¹ cell⁻¹, based on counts of $1.3 \pm 0.3 \times 10^6$ cells per particle, at peak growth, 40 h post-inoculation, $n = 3$). The background consumption rate obtained from the no-bacteria control (blue curve) was subtracted from the bacterial respiration rate. **(c)** *Vibrio cyclitrophicus* ZF270 uses membrane-bound/periplasmic alginate lyases for growth on alginate. Images of *Vibrio* colonies grown on a 0.5% alginate-containing agar plate. Alginate lyase secretion by *Vibrio splendidus* FF6 (lower panel) leads to the formation of a transparent ring (marked with arrows) on the opaque plate due to degradation of alginate. This ring is absent around the *Vibrio cyclitrophicus* ZF270 colony (upper panel), indicating that this strain does not secrete alginate lyase into the surrounding medium.

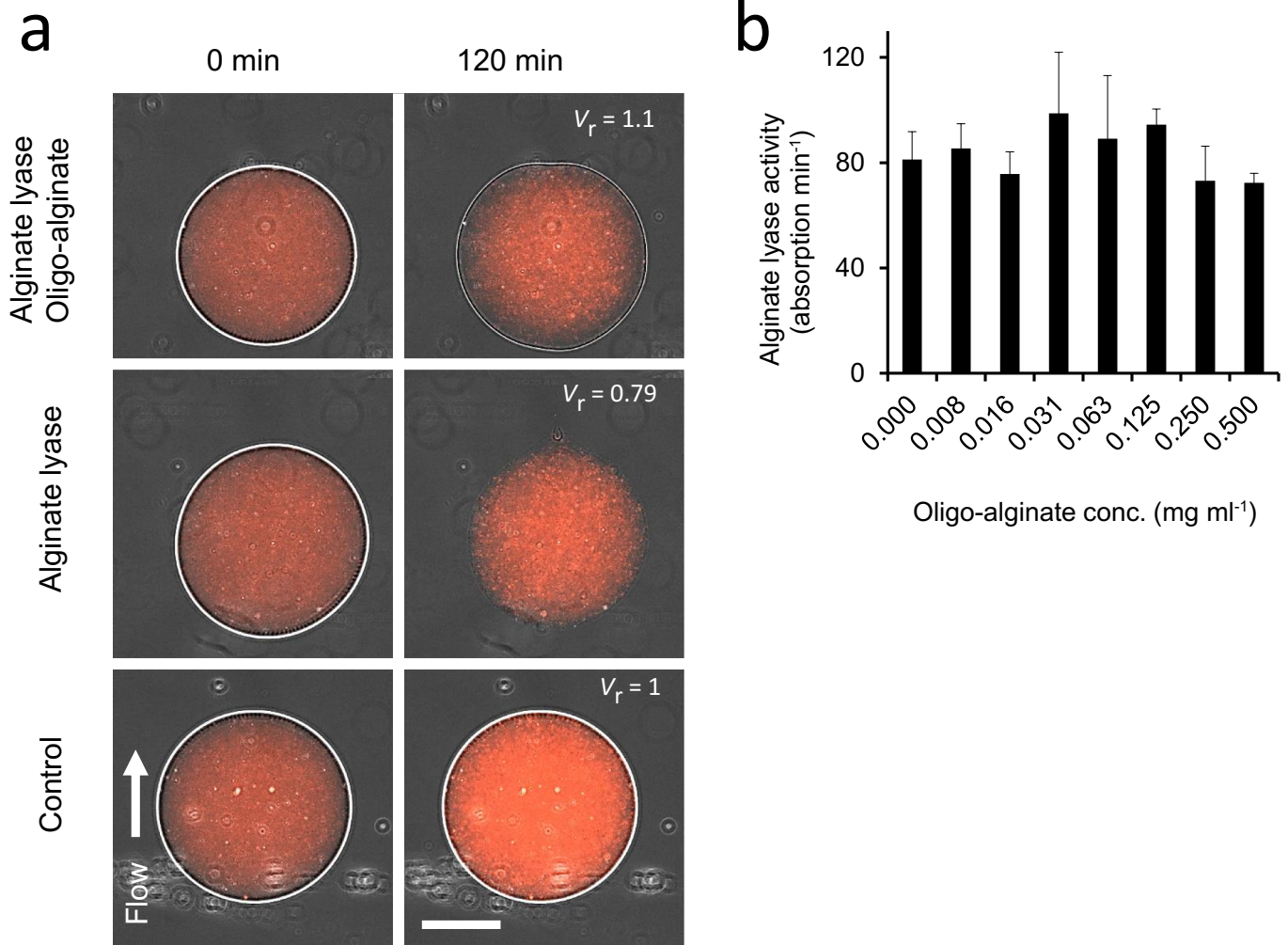


Extended Data Fig. 2 | Raman microscopy of alginate particles during degradation by *Vibrio cyclitrophicus* ZF270 suggests an accumulation of oligo-alginate on the surface of the particle even at intermediate flow rates during bacterial degradation, consumption and growth. (a, b) Stitched bright-field microscopy images ($22 \times 30 = 660$ and $29 \times 35 = 1,015$ images per picture) of a degraded particle (**a**; 42 h post-inoculation with bacteria) and a control particle (**b**; sterile particle). A flow rate of 7.25 m day^{-1} was imposed in both experiments. (**c, d**) Raman images of the spatial distribution of the carboxyl group (COOH) at the mid plane of the particle. Carboxyl groups are found on the mannuronate and guluronate subunits of alginate. The Raman map of the carboxyl group ($I_{1390-1440}$; integrated intensity in the spectral region $1390\text{--}1440 \text{ cm}^{-1}$) was normalized by the background intensity from the glass slide ($I_{520-570}$). Soluble oligo-alginate, the product of bacterial degradation, diffuses into and out of the particle and results in a higher Raman signal (**c**). The Raman signal of the carboxyl ion, indicating the presence of dissolved oligo-alginate, was highest around the periphery of the particle, and decreased towards the particle centre. In contrast, the spatial distribution of the carboxyl ion in the absence of bacterial degradation was homogeneous (**d**). The white circle represents the boundary of the alginate particle. Panels (**c**) and (**d**) are stitched images with $20\text{-}\mu\text{m}$ step size in x - and y -directions. Scale bars: $100 \mu\text{m}$.

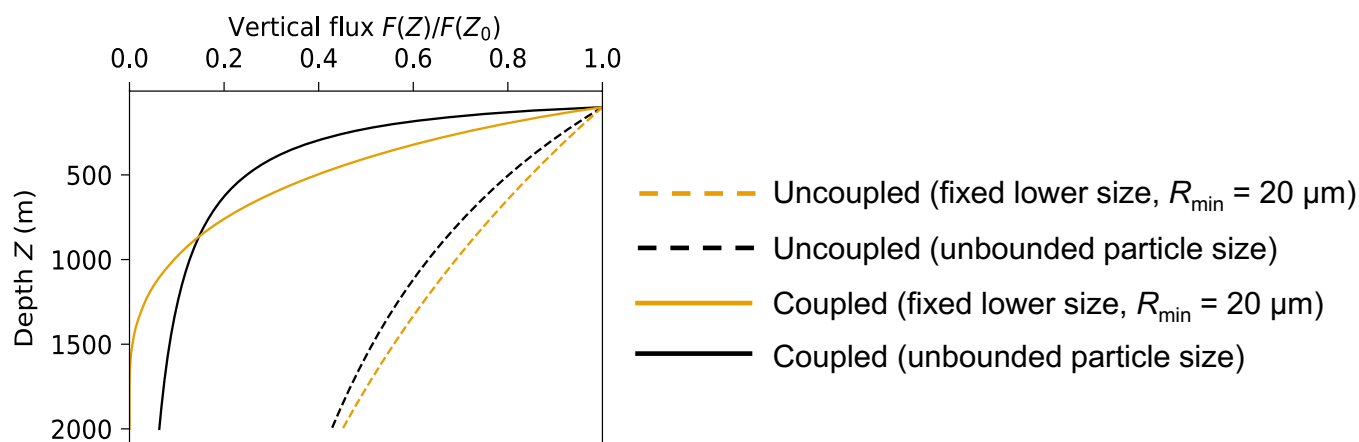
T = 30 h



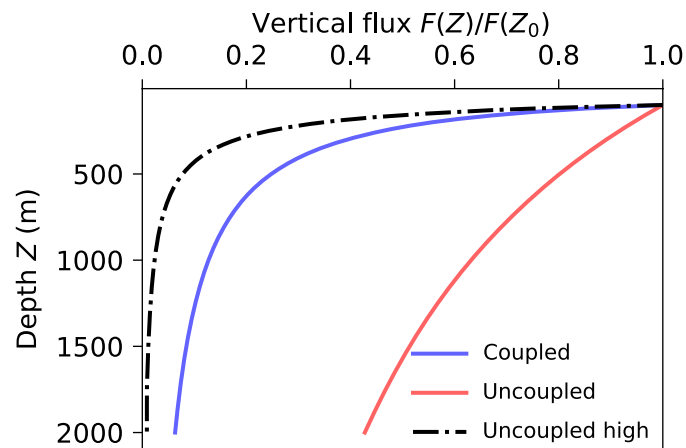
Extended Data Fig. 3 | *Vibrio cyclitrophicus* ZF270 biofilms on particles 30 h post-inoculation in flow of different concentrations of oligo-alginate or in 1% marine broth 2216. Bacterial degradation was monitored under a flow of 7.25 m day^{-1} of medium supplemented with different concentrations of oligo-alginate or with 1% marine broth 2216 (complementary control; see main text). White arrows indicate bacterial biofilms, which form in oligo-alginate concentrations $\geq 0.04 \text{ mg ml}^{-1}$ and in 1% marine broth 2216. Although more cells reside on particles at higher oligo-alginate concentrations, the degradation rate is lower than at lower oligo-alginate concentrations. For example, upon addition of 0.04 mg ml^{-1} oligo-alginate, the biofilm thickness was $33 \pm 11 \mu\text{m}$ and the degradation rate was $(7.5 \pm 0.1) \times 10^{-3} \text{ mm}^3 \text{ h}^{-1}$, whereas for zero addition of oligo-alginate, the biofilm thickness was $8 \pm 3 \mu\text{m}$ and the degradation rate was $(20.5 \pm 0.8) \times 10^{-3} \text{ mm}^3 \text{ h}^{-1}$. Scale bar: $400 \mu\text{m}$.



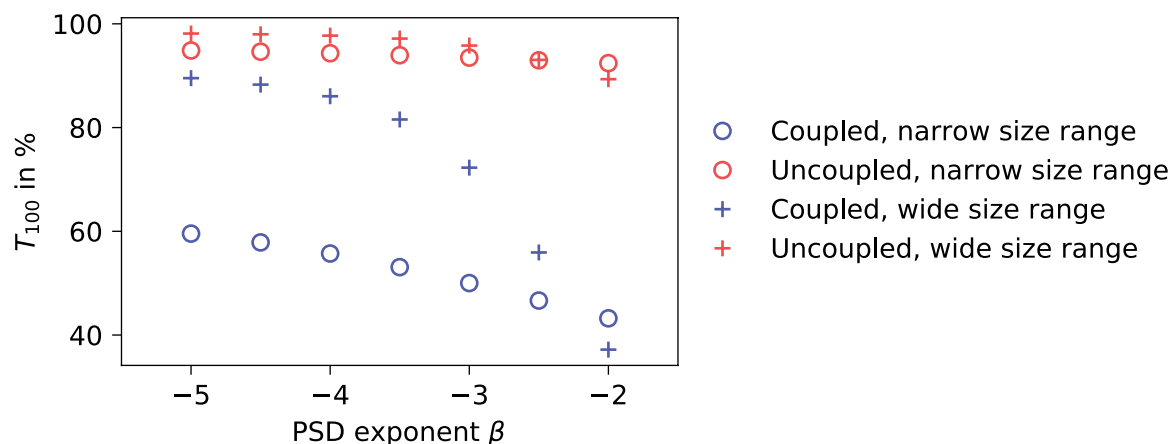
Extended Data Fig. 4 | High concentrations of oligo-alginate inhibit the degradation of alginate particles but do not affect alginate lyase activity. (a) Particles exposed to alginate lyase enzyme under a flow rate of 7.25 m day^{-1} for 120 min in the presence or absence of 1 mg ml^{-1} oligo-alginate $<10 \text{ kDa}$ (see also Supplementary Movie 4). An experiment with 1 mg ml^{-1} oligo-alginate but with no alginate lyase enzyme is presented as a negative control. Degradation of the particle is only detected in the presence of alginate lyase but the absence of oligo-alginate. The volume of the particle relative to time zero (V_r) is indicated within each panel. Scale bar: $400 \mu\text{m}$. **(b)** Addition of oligo-alginate does not inhibit the activity of alginate lyase. Alginate lyase activity was measured by monitoring the increase in absorption at 235 nm using a plate reader. Reactions were performed in 10 mM MOPS buffer containing $20 \mu\text{g ml}^{-1}$ alginate lyase, 0.1% (w/v) sodium alginate, 2 mM CaCl_2 and the concentrations of oligo-alginate $<10 \text{ kDa}$ given on the x axis (see Methods). No differences in enzyme activity were observed across the range of concentrations tested ($n=3$ for each value of concentration).



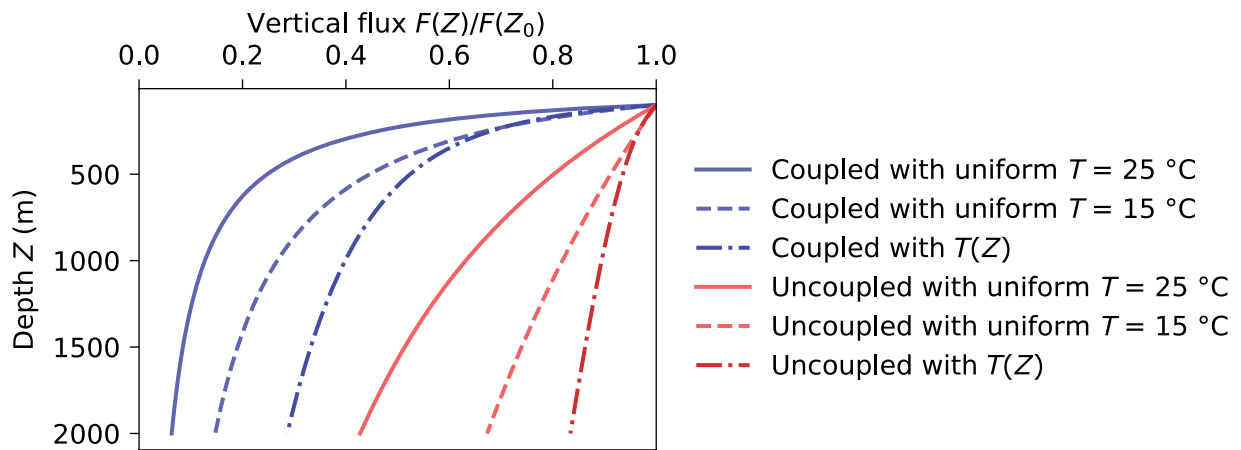
Extended Data Fig. 5 | The coupling of sinking speed and degradation rate in models that consider a fixed minimum particle size. Shown is the vertical flux of POC as a function of depth, $F(Z)$, normalized by its value $F(Z_0)$ at the euphotic layer depth, $Z_0 = 100$ m, predicted by our model when accounting for the observed coupling of sinking and degradation (continuous curves) or when excluding this coupling (reference case, dashed curves). When assuming a fixed lower bound, $R_{\min} = 20 \mu\text{m}$, for the radius of particles contributing to the flux (orange curves), our model shows a similar trend to the results presented in Fig. 4 (here shown with black curves), for which the range of radii varies with depth as particles are degraded. The minimum size was chosen by considering the experimental lower bound of the size of particles that can be detected by vision profilers with a fixed lower resolution^{35,51}, to represent the lower bound on particles that are considered in empirical estimates of the POC flux. In both of the coupled approaches (continuous curves), the coupling of sinking speed with degradation results in a faster decrease of the vertical flux with depth compared to the reference case that neglects the coupling. All curves were derived from the following initial conditions: total concentration $200 \text{ particles l}^{-1}$ at initial depth $Z_0 = 100$ m, with a PSD slope of -4 over particles with initial radii in the range $125\text{--}750 \mu\text{m}$ for the varying range assumption (black) and initial radii $20\text{--}750 \mu\text{m}$ for the fixed lower bound assumption (orange).



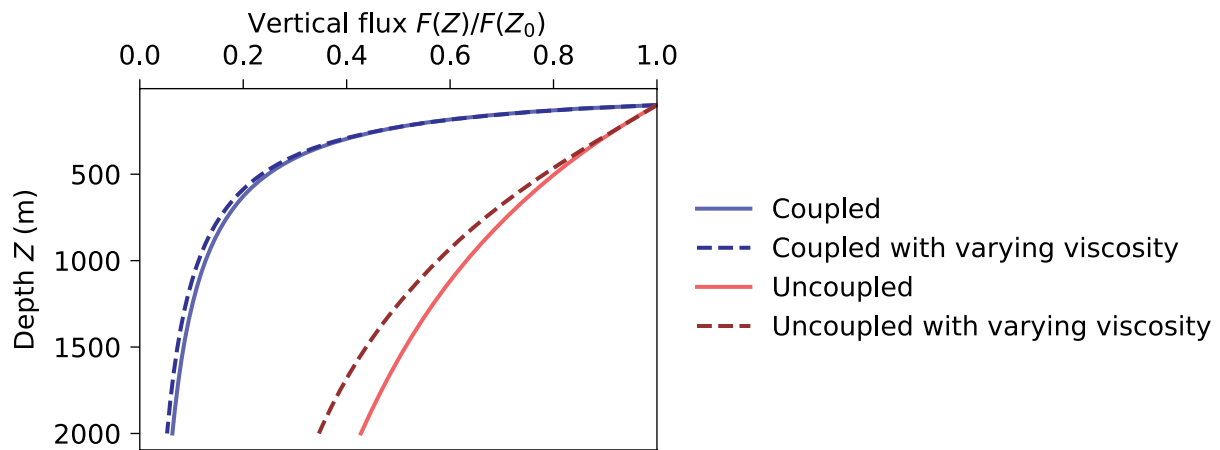
Extended Data Fig. 6 | Comparison of results from models incorporating the coupling of sinking and degradation with a reference case imposing a fixed high degradation rate for all particles. Shown is the vertical flux of POC as a function of depth, $F(Z)$, normalized by its value $F(Z_0)$ at the euphotic layer depth, $Z_0=100$ m, predicted by our model when accounting for the observed coupling of sinking and degradation (blue curve) or when excluding this coupling (reference case, red curve). Also shown are results from a variant of the reference case that considers a uniform high rate of shrinking of the radius over the entire range of particle sizes (dash-dotted curve), corresponding to the initial shrinking rate of the largest particle considered at the initial depth Z_0 ($R_0=750\ \mu\text{m}$) in the coupled case. All curves were derived from the following initial conditions: total concentration $200\ \text{particles l}^{-1}$ at initial depth $Z_0=100$ m and a PSD slope of -4 over particles of radii ranging between 125 and $750\ \mu\text{m}$. Note that the uncoupled high degradation case (dash-dotted curve) assumes a constant degradation rate that was measured under high flow, thus it overestimates the degradation compared to the coupled dynamics (blue curve).



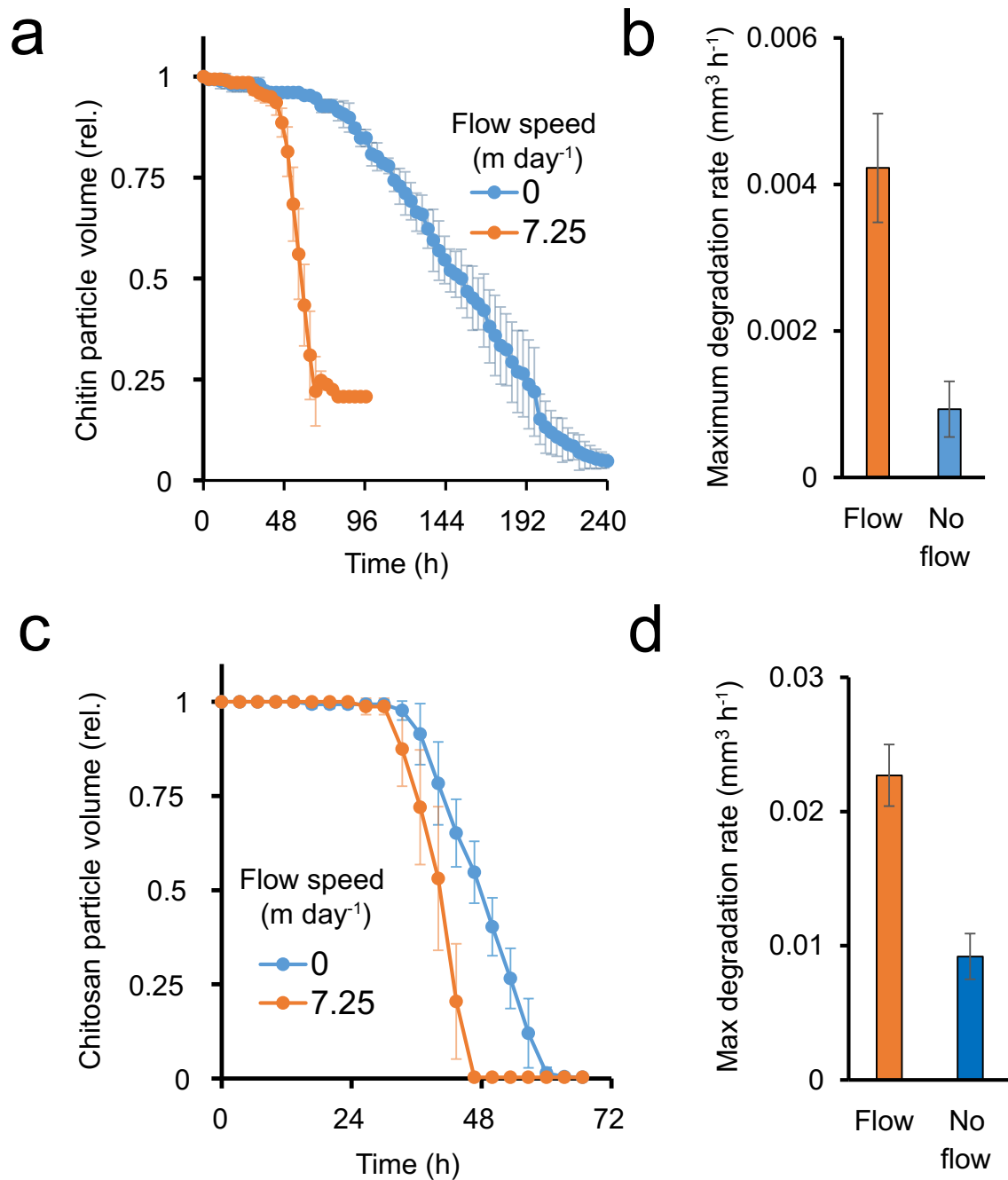
Extended Data Fig. 7 | Sensitivity of sinking-enhanced degradation to the characteristics of the particle size distribution (PSD). Using our model, we computed the transfer efficiency of the vertical flux of POC to a depth of 100 m below the euphotic zone, denoted T_{100} , that is $T_{100} = F(Z_0 + 100)/F(Z_0)$ with $Z_0 = 100$ m the depth of the euphotic zone, for different PSDs covering the range of existing oceanic regimes. By varying the PSD slope from -5 to -2, we move from typical oligotrophic PSDs dominated by small particles to typical eutrophic PSDs where larger particles are more prominent and can dominate in volume. For each PSD slope, we also considered a narrow range of initial particle size ($R_0 = 125$ to $750 \mu\text{m}$, circles), and a wider range representative of extended capabilities of Underwater Video Profilers to detect particles⁵¹ ($R_0 = 22.5$ to $2500 \mu\text{m}$, crosses). For each set of initial conditions, we ran our model including the sinking-enhanced degradation mechanism (coupled case, in blue) and without the coupling as a null model (uncoupled, in red). These results demonstrate that as the PSD skews towards small particles with slope closer to -5, typical of oligotrophic regions, the difference in flux between the uncoupled and coupled models becomes smaller. In contrast, a PSD with a greater contribution from large particles, with slope close to -2 like that in eutrophic regions, results in a greater difference between the coupled and uncoupled models. This is intuitive given the stronger enhancement of degradation for larger particles resulting from their faster sinking. In the same manner, we observe that including a wider range of particle sizes in the distribution for oligotrophic regions (with slopes -5 to -4) results in a weaker effect of the coupling of sinking and degradation on the POC flux, through the dominant contribution of very small particles. In contrast, the same wider range of particle sizes reinforces the effect of coupling in eutrophic regions (with PSD slopes of -2), where larger particles make a dominant contribution to the flux.



Extended Data Fig. 8 | Modelling the coupling of sinking and degradation while including the effect of the water column temperature gradient on degradation rate. Shown is the vertical flux of POC as a function of depth, $F(Z)$, normalized by its value $F(Z_0)$ at the euphotic layer depth, $Z_0 = 100$ m. Continuous curves account for the observed coupling of sinking and degradation (blue continuous curve) or exclude this coupling (reference case, red continuous curve), as in Fig. 4, for estimates of degradation rate at temperature $T = 25\text{ }^\circ\text{C}$. The degradation rates of both coupled and uncoupled cases were also modelled while considering the reduction of degradation rate with decreasing temperature, assuming a reduction by a factor 2.5 for each $10\text{ }^\circ\text{C}$ decrease in temperature, (i.e. temperature coefficient $Q_{10} = 2.5$). The results are presented for two alternative assumptions: 1) the degradation rate is uniform over the water column but corresponds to a temperature $T = 15\text{ }^\circ\text{C}$ (dashed curves); 2) a fitted temperature profile $T(Z)$ for subtropical waters (see equation (17) Supplementary Information) modulates degradation over the water column (dash-dotted curves). For both assumptions, red curves correspond to the uncoupled reference case while blue curves correspond to the sinking-degradation coupled case. All curves were derived from the following initial conditions: total concentration $200\text{ particles l}^{-1}$ at initial depth $Z_0 = 100$ m and a PSD slope of -4 over particles of radii ranging between 125 and $750\text{ }\mu\text{m}$. As our experimental degradation rate was measured at $T = 25\text{ }^\circ\text{C}$, the reduction of degradation rate imposed by considering $T = 15\text{ }^\circ\text{C}$ or a complex profile $T(Z)$ both result in a weaker attenuation of the flux with depth. However, note that regardless of this effect of temperature, there remains a strong attenuation of POC flux with sinking-degradation coupling with respect to the reference uncoupled case.



Extended Data Fig. 9 | Varying viscosity with seawater temperature has only a minor effect on the modelled POC flux. Shown is the vertical flux of POC as a function of depth, $F(Z)$, normalized by its value $F(Z_0)$ at the euphotic layer depth, $Z_0 = 100$ m, predicted by our model when accounting for the observed coupling of sinking and degradation (blue continuous curve) or when excluding this coupling (reference case, red continuous curve), as in Fig. 4. Also shown are results from models in which seawater viscosity varies with temperature, both in the coupled (dark blue dashed curve) and uncoupled case (dark red dashed curve). The temperature profile corresponds to subtropical waters with a sharp decrease with depth (see equation (17) Supplementary Information). All curves were derived from the following initial conditions: total concentration $200 \text{ particles l}^{-1}$ at initial depth $Z_0 = 100$ m and a PSD slope of -4 over particles of radii ranging between 125 and $750 \mu\text{m}$.



Extended Data Fig. 10 | Flow plays a key role in determining bacterial degradation of chitin and chitosan particles. (a,c) Time series of particle volume during bacterial degradation of chitin (a) and short-chain chitosan (c) particles under flow of 7.25 m day⁻¹ and under no-flow conditions (shown relative to initial volume; mean and SD; $n=3$ replicate experiments, except for flow in (a) for which $n=4$). (b,d) Maximum degradation rate of chitin (b) and chitosan (d) particles. The apparent degradation rate is ~4-fold faster (chitin) or ~2.5-fold faster (chitosan) in flow compared to no-flow conditions. Note that the degradation rate estimated from volume loss in the case of chitin and chitosan is only a proxy for the mass loss, since *Vibrio splendidus* (1A01) and *Psychromonas* (6C06) degrade the particle using membrane-bound enzymes but possibly also by using secreted enzymes^{52,53}. Thus, unlike the case for alginate, degradation may occur from within the particle as well as on the surface, so that measurements of volume reduction may underestimate degradation rate. Flow speed in all panels is represented by colour; blue – no flow, orange – flow speed of 7.25 m day⁻¹. Movies showing the degradation dynamics can be provided by the authors upon request.